

Article

On the nature and distribution of mineral-forming ions: A mineral informatics approach

Hallimond Lecture

Marko Bermanec¹ , Jiyin Zhang² , Robert T. Downs³, Dominik Kunić⁴, Xiaogang Ma², Shaunna M. Morrison^{5,6}, Anirudh Prabhu⁶ and Robert M. Hazen⁶

¹Department of Earth Sciences, University of Graz, Graz, Austria; ²Department of Computer Sciences, University of Idaho, Moscow, ID, USA; ³Department of Geological Sciences, University of Arizona, Tucson AZ, USA; ⁴Department of Geology, Faculty of Science, University of Zagreb, Zagreb, Republic of Croatia; ⁵Department of Earth and Planetary Sciences, Rutgers University New Brunswick, Wright-Rieman Laboratories, Piscataway, NJ, USA; and ⁶Earth and Planets Laboratory, Carnegie Institution for Science, Washington DC, USA

Abstract

Minerals incorporate 72 different essential elements, many of which are redox sensitive. We compiled oxidation states of ions in 4834 IMA-approved mineral species with oxygen and/or halogens as anions and have identified 87 essential mineral-forming ions. We compiled data on the coexistence of these ions as recorded in their minerals' chemical formulas, and applied methods of network analysis with community detection and heatmap analysis with agglomerative clustering to reveal patterns of ion coexistence.

Unipartite networks illustrate the most common coexisting ion pairs, whereas Louvain and Walktrap methods reveal distinct ion groups—patterns that both reinforce and refine the Goldschmidt geochemical classification of elements. Key findings include: (1) that mineral-forming ions group into two major communities with a number of subcommunities; (2) that different ion communities primarily reflect contrasting geochemical and paragenetic processes such as primary igneous mineralisation, hydrothermal precipitation, and near-surface oxidation and weathering, rather than crystal chemical constraints; and (3) that different oxidation states of some redox-sensitive elements fall into two or more of these communities, underscoring how ions of the same elements commonly display contrasting geochemical and/or paragenetic affinities.

Heatmap analysis reveals groupings of co-occurring ions that mimic many aspects of community detection methods, as well as significant patterns of ion antipathies—groups of ions that are seldom if ever paired. For example, alkali metals commonly associated with late-stage igneous fluids (Cs^+ , Li^+ and Rb^+) rarely co-occur with low field strength ions found concentrated in brines (Ag^+ , Br^- , Cu^+ , Hg^+ and I^-) or high field strength ions from weathered primary oxide or sulfide deposits (Cr^{6+} , Pb^{4+} , Mo^{4+} , Te^{4+} and Te^{6+}). Such ion pairs are well known in synthetic oxides. Therefore, with the exceptions of cations having very different redox potentials, unobserved ion pairs are principally the consequences of element rarity coupled with natural geochemical and paragenetic antipathies rather than crystal chemical constraints.

Keywords: network analysis; heatmap analysis; oxidation states; element classification; paragenetic modes

(Received 17 February 2025; revised 29 May 2025; accepted 29 May 2025; Accepted Manuscript published online: 11 July 2025)

Introduction

Patterns in the diversity and distribution of mineral-forming elements have pointed to systematic trends in the chemical character of these elements, as proposed by the Goldschmidt geochemical classification (Goldschmidt, 1937; Moore *et al.*, 2022; Hummer

Corresponding author: Robert M. Hazen; Email: rhazen@carnegiescience.edu Associate Editor: Andrew G. Christy

This paper is part of a collection in tribute to the work of Edward Grew at 80

Cite this article: Bermanec M., Zhang J., Downs R.T., Kunić D., Ma X., Morrison S.M., Prabhu A. and Hazen R.M. (2025) On the nature and distribution of mineral-forming ions: A mineral informatics approach. *Mineralogical Magazine*, 1–15. https://doi.org/10.1180/mgm.2025.10105

et al., 2023; Lodders and Hazen, 2026). This useful classification model groups elements into one of four preferred hosts phases, including siderophile (in iron and other metals), chalcophile (in sulfides and other chalcogenides), lithophile (in oxygen-based rocks), and atmophile (in the atmosphere as gases). Most mineral-forming elements occur predominantly with other elements in their geochemical group.

As Goldschmidt emphasised, many elements, especially those with multiple oxidation states, have affinities for more than one host. For example, iron occurs as a siderophile native element and as chalcophile or lithophile Fe²⁺ and Fe³⁺ ions (e.g. Wood and Kiseeva, 2015). Recent efforts to expand mineral formulas to include oxidation states (see https://rruff.info/ima/#, accessed 05

February 2025; Lafuente *et al.*, 2015) have resulted in the tabulation of ions in most mineral species. Thus, for example, the iron-bearing olivine fayalite (Fe₂SiO₄) is recast as Fe²⁺₂Si⁴⁺O²⁻₄. The resulting formulas offer the opportunity to expand the Goldschmidt approach by identifying the preferred host phases for redox-sensitive, mineral-forming ions in these minerals. Furthermore, the availability of the comprehensive RRUFF and Mindat (https://mindat.org, accessed 05 February 2025) data resources, coupled with mineral informatics methods of network analysis with community detection and heatmap analysis with agglomerative clustering, offer a rigorous, data-driven approach to this problem.

Mineral-forming ions

The concept of a mineral-forming 'ion' is a flawed but useful fiction. Despite the common description of many mineral structures in terms of ionically bonded cations and anions, theoretical models and experimentally determined electron density studies demonstrate that the chemical bonds in oxide and sulfide minerals feature both significant ionic and covalent aspects (Pauling, 1960; Gibbs *et al.*, 2014). For example, Si–O bonds in silicates, C–O bonds in carbonates and S–O bonds in sulfates are intermediate on the spectrum between predominantly ionic (i.e. with the transfer of electron density from the cation/metal to the anion/oxygen), such as Na–Cl bonds in halite (NaCl), and predominantly covalent (i.e. sharing of electron density across the bond), as in As–S bonds in orpiment (As₂S₃).

One can employ relative electronegativities (Pauling, 1932), χ , to assign cations versus anions, as well as to estimate the relative ionicity of those bonds. For example, Na⁺ ($\chi=0.93$) is the positively-charged cation relative to the anion Cl⁻ ($\chi=3.16$); the relatively large electronegativity difference of 2.23 units suggests a predominantly ionic bond in halite (Na⁺Cl⁻). Similarly, As³⁺ ($\chi=2.18$) is the cation relative to S²⁻ ($\chi=2.58$) in the arsenic sulfide orpiment (As³⁺₂S²⁻₃), though the 0.40 difference in electronegativity is significantly less than in NaCl and points to a predominantly covalent bond.

In this study we focus on ions that co-exist in a mineral (as opposed to ions directly bonded to each other), as recorded in each mineral's chemical formula using the International Mineralogical Association (IMA) approved formulae at https://rruff.info/ima/# (accessed 5 February 2025). We only consider minerals with anions O²⁻ and/or halogens (F⁻, Cl⁻, Br⁻, I⁻), as well as select minerals with C⁴⁻, N³⁻, or S²⁻. Consequently, we do not include several important mineral groups with likely metal-metal, cation-cation, or anion-anion bonding, including native elements; predominantly covalently bonded sulfides, arsenides and other chalcogenides; sulfosalts; hydrocarbon minerals; or borides, carbides, nitrides, phosphides and silicides. These restrictions result in the removal in this study of eight noble metal elements (Au, Ir, Os, Pd, Pt, Re, Rh and Ru) from the list of 72 mineral-forming elements.

We acknowledge that nominal oxidation states can be informative even in the case of minerals with non-ionic bonding. For example, the reaction of pyrite (FeS₂) to pyrrhotite (Fe₇S₈) requires a change in the number of bonded electrons, because Fe remains effectively Fe²⁺ but a portion of S transitions from S¹⁻ to S²⁻ (Letard *et al.*, 2007, and references therein). Even though the distribution of electrons is not strongly centred around a given Fe or S atom, owing to nearly metallic bonding, the nominal oxidation states still reveal how the electron distribution is different between different

materials. The problem with including most sulfides and sulfosalts is that for many of these minerals the nominal oxidation state is unknown or highly debated (e.g. Pearce *et al.*, 2006). Therefore, trying to include them in this study would add uncertainties to the dataset that are not present in minerals with oxygen or halogens as anions.

These constraints result in 4834 IMA-approved minerals for which the oxidation states of 64 essential chemical elements, including 87 different ions, are unambiguously defined (Table 1). Among the characteristics of these ions and ion pairs:

- (1) The 25 most common ions in the 4834 mineral species considered, all with more than 250 occurrences, are O^{2-} (4741), H^+ (3230), Si^{4+} (1618), Ca^{2+} (1428), Al^{3+} (1157), Na^+ (1107), Fe^{3+} (740), Mg^{2+} (738), P^{5+} (701), S^{6+} (609), K^+ (545), Mn^{2+} (545), Fe^{2+} (488), Cu^{2+} (467), As^{5+} (463), F^- (458), Cl^- (405), Ti^{4+} (391), C^{4+} (381), Pb^{2+} (372), P^{3+} (302), P^{3+} (283), P^{3+} (279), P^{3+} (274) and P^{3+} (260).
- (2) By contrast, four of the 87 ions (C^{4-} , Hf^{4+} , I^{3+} and V^{2+}) have been recorded in only one mineral species, whereas two ions (In^{3+} and S^{2+}) occur only twice in our compilation. (Note that, though ' S^{2+} ' is a useful way to designate thiosulfate, the thiosulfate ion in fact incorporates equal numbers of S^{6+} and S^{2-}).
- (3) The majority of the 87 mineral-forming ions are cations, including 1^+ (10 examples), 2^+ (17), 3^+ (18, including 'REE³⁺', which lumps all species-determining trivalent rare earth elements), 4^+ (17), 5^+ (10) and 6^+ (7).
- (4) Of the 87 mineral-forming ions tabulated, eight are anions, including 1 $^-$ (F $^-$, Cl $^-$, Br $^-$, I $^-$), 2 $^-$ (O 2 -, S 2 -), 3 $^-$ (N 3 -), and 4 $^-$ (C 4 -).
- (5) Most ion pairs never form. With 87 different mineral-forming ions, there exists 3741 {i.e. $[(87 \times 87) 87]/2$ } possible pairs between two different ions. However, only 1392 (37.2%) of these possible pairs are found to co-occur one or more times in the 4834 minerals in our survey. Furthermore, 280 of those observed pairs (20.1% of the 1392) are only found in one mineral.
- (6) The five most commonly co-occurring ions are also bonded cation– O^{2-} pairs, including: H^+-O^{2-} (3222 pairs), $Si^{4+}-O^{2-}$ (1611), $Ca^{2+}-O^{2-}$ (1412), $Al^{3+}-O^{2-}$ (1139), and Na^+-O^{2-} (1084), with significant co-occurrence of $Fe^{3+}-O^{2-}$ (735), $Mg^{2+}-O^{2-}$ (731), $P^{5+}-O^{2-}$ (699), and $S^{6+}-O^{2-}$ (607). The most commonly co-occurring pairs of cations (not bonded pairs) are $Si^{4+}-H^+$ (1058), $Ca^{2+}-H^+$ (985), Na^+-H^+ (719), $Mg^{2+}-H^+$ (719), $Al^{3+}-H^+$ (880), $Ca^{2+}-Si^{4+}$ (699), and $Al^{3+}-Si^{4+}$ (618), while the most common co-occurring anion-anion pairs (also not bonded) are $O^{2-}-F^-$ (407) and $O^{2-}-Cl^-$ (367).

Methods

Employing data recorded at https://rruff.info/ima/# (accessed 5 February 2025), we compiled an xlsx spreadsheet with 4834 rows, each representing a different mineral species approved by the International Mineralogical Association's Committee on New Minerals, Nomenclature, and Classification (IMA-CNMNC; Burke 2006; Mills *et al.*, 2009; Schertl *et al.*, 2018), and 87 columns, each representing a different mineral-forming ion (Supplementary Table 1).

The case of trivalent rare earth elements deserves special attention, because official IMA formulas for REE minerals are inconsistent. In some cases (at least 36 instances) 'REE' appears in an approved mineral formula. In two additional minerals, aeschynite-Nd and aeschynite-Y, the symbol 'Ln', presumably for 'lanthanide',

Table 1. Distribution of 87 mineral-forming ions among Clusters and Communities

lon	# Minerals*	Heatmap Cluster	Louvain	Walktrap	Electro- negativity	lon	# Minerals*	Heatmap Cluster	Louvain	Walktrap	Electro- negativity
Ag^+	12	E	2	2	1.93	N ³⁻	95	Α	2	2	3.04
Al^{3+}	1157	F	1	1	1.61	N^{5+}	20	Α	2	2	3.04
As^{3+}	79	В	3	1	2.18	Na^+	1107	G	1	1	0.93
As^{5+}	463	Α	4	2	2.18	${\rm Nb^{5+}}$	158	G	1	1	1.60
B^{3+}	302	В	1	1	2.04	Ni^{2+}	84	Α	3	5	1.91
Ba^{2+}	260	В	1	1	0.89	O ²⁻	4741	-	-	-	3.44
Be^{2+}	130	В	1	1	1.57	P^{5+}	701	В	1	1	2.19
Bi ³⁺	89	Α	3	3	2.02	Pb^{2+}	372	F	2	2	1.87
Br-	10	E	2	2	2.96	Pb^{4+}	6	E	2	2	1.87
C^{4+}	381	В	1	1	2.55	REE ³⁺	274	G	1	1	1.2***
C ⁴⁻	1	F	-**	-	2.55	Rb^+	3	D	1	1	0.82
Ca^{2+}	1428	G	1	1	1.00	S ²⁻	2	E	2	4	2.58
Cd^{2+}	15	С	3	2	1.69	S^{2+}	22	F	2	2	2.58
Ce ⁴⁺	6	В	1	1	1.12	S ⁴⁺	22	В	1	1	2.58
Cl-	405	F	2	2	3.16	S^{6+}	609	С	3	2	2.58
Co^{2+}	41	Α	3	2	1.88	Sb^{3+}	39	E	2	4	2.05
Co^{3+}	6	Α	3	5	1.88	Sb ⁵⁺	60	В	4	1	2.05
Cr ³⁺	61	В	1	1	1.66	Sc ³⁺	23	В	1	1	1.36
Cr ⁶⁺	26	E	2	2	1.66	Se ⁴⁺	42	С	2	2	2.55
Cs ⁺	25	D	1	1	0.79	Se ⁶⁺	6	С	2	2	2.55
Cu ⁺	15	E	2	2	1.90	Si ⁴⁺	1618	G	1	1	1.90
Cu ²⁺	467	С	2	2	1.90	Sn ²⁺	6	E	5	7	1.96
F-	458	D	1	1	3.98	Sn ⁴⁺	41	В	1	1	1.96
Fe ²⁺	488	G	1	1	1.83	Sr ²⁺	156	G	1	1	0.95
Fe ³⁺	740	В	4	1	1.83	Ta ⁵⁺	58	E	5	7	1.50
Ga ³⁺	4	Α	2	2	1.81	Te ⁴⁺	54	Е	4	2	2.10
Ge ⁴⁺	15	Α	2	2	2.01	Te ⁶⁺	52	Е	2	2	2.10
H ⁺	3220	-	-	-	2.20	Th ⁴⁺	37	В	1	1	1.30
Hf ⁴⁺	1	С	-	-	1.30	Ti ³⁺	10	D	1	1	1.54
Hg ⁺	19	E	2	2	2.00	Ti ⁴⁺	391	G	1	1	1.54
${\rm Hg^{2+}}$	20	F	2	2	2.00	Tl ⁺	11	Α	3	2	1.62
I-	14	Е	2	2	2.66	Tl ³⁺	4	С	2	2	1.62
I ³⁺	1	F	-	-	2.66	U ⁴⁺	32	В	1	1	1.38
I ⁵⁺	12	E	2	1	2.66	U ⁵⁺	3	С	6	6	1.38
In ³⁺	2	Α	-	-	1.78	U ⁶⁺	283	С	6	6	1.38
K ⁺	545	С	1	1	0.82	V ²⁺	1	F	-	-	1.63
Li ⁺	123	D	1	1	0.98	V ³⁺	43	В	1	1	1.63
Mg ²⁺	738	В	1	1	1.31	V ⁴⁺	66	A	3	1	1.63
Mn ²⁺	508	В	4	1	1.55	V ⁵⁺	189	A	3	1	1.63
Mn ³⁺	108	В	4	1	1.55	W ⁶⁺	47	В	4	-	2.36
Mn ⁴⁺	39	В	4	1	1.55	γ3+	132	В	1	1	1.22
Mo ⁴⁺	5	E	-	-	2.16	Zn ²⁺	279	В	3	2	1.65
Mo ⁵⁺	3	С	3	3	2.16	Zr ⁴⁺	142	G	1	1	1.33
Mo^{6+}	69	С	3	3	2.16						

^{*}Based on a survey of 4834 minerals; see Supplementary Table 1.

appears in the formula. However, in many other minerals the formula specifies a dominant rare earth element, including Ce^{3+} (167 minerals), Dy^{3+} (1), Er^{3+} (1), Gd^{3+} (2), La^{3+} (63), Nd^{3+} (34), Sm^{3+} (2), and Yb^{3+} (5). Given that all 14 stable rare earth elements in the 3+ oxidation state will co-occur in all these mineral species, we have combined these varied instances in the data analysis process into one ion—REE³⁺. In addition, note that six occurrences of Ce^{4+} are treated separately in this study (see Supplementary Tables 1, 2 and 3).

Unipartite network analysis and Louvain community detection of coexisting ions

A principal objective of this study is to apply community detection and agglomerative clustering to discern patterns in the co-occurrence of mineral-forming ions. Network analysis reveals communities of associated members of a group, whether people in a social setting or minerals in a natural assemblage, through links between nodes (Kolaczyk, 2009; Newman, 2013; Morrison *et al.*, 2017; Hazen *et al.*, 2023a). Each node represents a member of the

^{**}Not included in this visualisation.

^{***}All trivalent lanthanide elements are lumped into REE $^{3+}$.

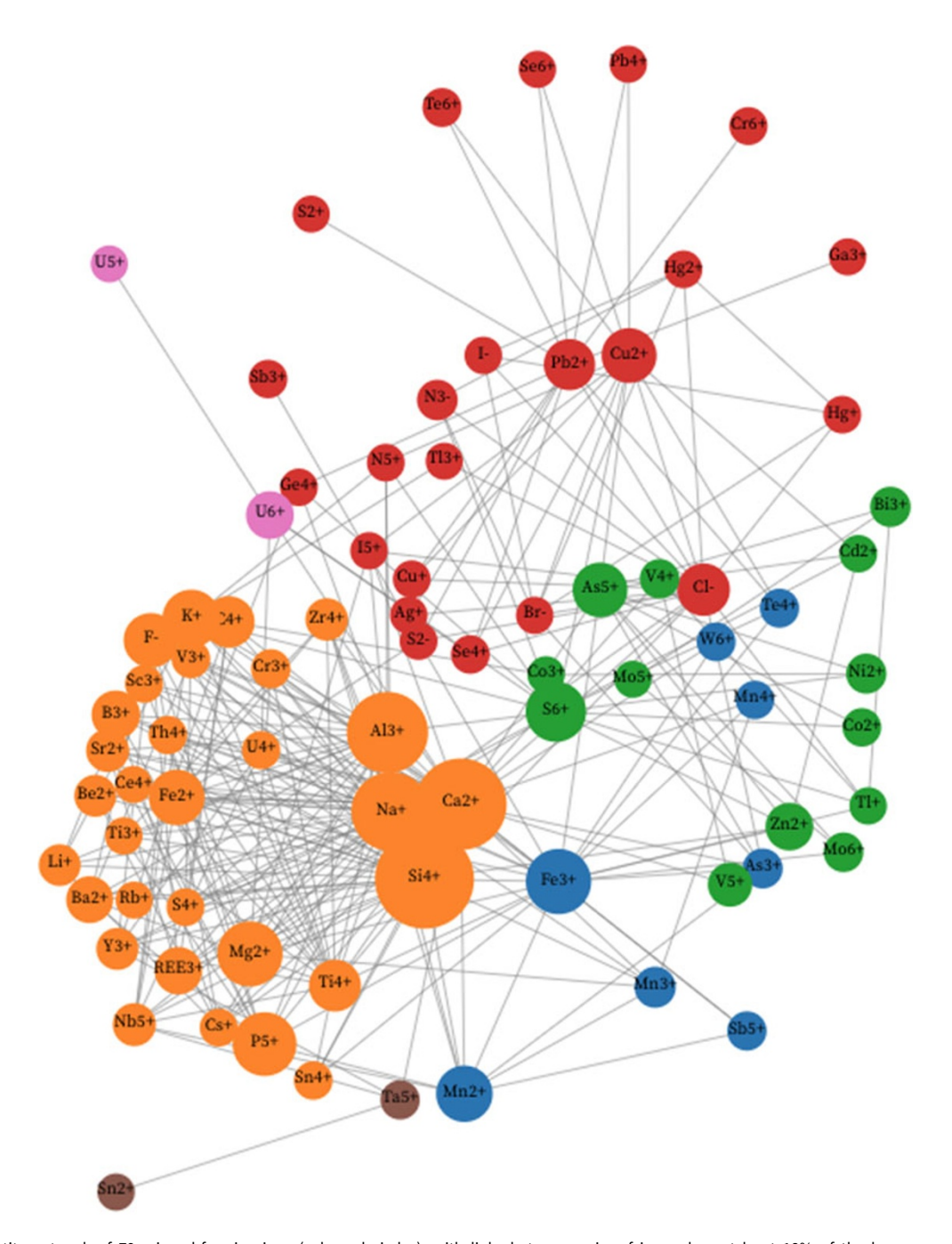


Figure 1. A unipartite network of 79 mineral-forming ions (coloured circles), with links between pairs of ions when at least 18% of the less common ion also occurs with the more common ion. Node sizes indicate the relative abundances of ions, while colours indicate six communities of ions that were determined using Louvain community detection (see text). Each of these six communities (see text) corresponds to groups of ions that co-occur relatively frequently. This figure is a static image of an interactive web-based graphic. One can vary the percentage cutoff for links between nodes by sliding 'lon Cutoff' vernier in the interactive version of this graph at https://observablehq.com/d/726edcffdbc8fecc. Slide the'lon cutoff by ABS to remove the least common ions, based on the absolute numbers of occurrences. Use the 'remove lon' feature to remove one or more ions from the network. Click and hold your cursor on any node to move that node and identify links to other nodes.

population, while each link represents an association between two nodes. Figure 1 displays a unipartite network that illustrates the coexistence of 79 mineral-forming ions, as listed in Table 1.

This graph was built on 'Observable' (https://observablehq.com/), using D3js (Bostock et al., 2011). The networks use the D3-force algorithm (https://d3-wiki.readthedocs.io/zh_CN/master/Force-Layout/) for its network layout. This force-directed graph treats edges between nodes as an array of interconnected

springs. The interactive network can be rotated into varied orientations; therefore, the visual distances between nodes will vary based on the projection employed. The code and an interactive version of this network can be found at: https://observablehq.com/d/726edcffdbc8fecc (for instructions, see Fig. 1 caption).

Each of the 79 nodes in Fig. 1 represents a mineral-forming ion. Note that eight of the 87 ions in Table 1 and Supplementary Table 1 are not incorporated as nodes in Fig. 1 to avoid skewing the results

and interpretation of network analysis. We apply two criteria for removing these eight ions:

- (1) We exclude the two most common ions, O^{2-} [found in 4741 (98.1%) of the 4834 minerals studied] and H^+ [in 3230 minerals (66.8%)]. These ions are so abundant as to span all potential network communities—a situation that significantly increases the density of the network while diminishing the discrimination among several communities.
- (2) We exclude six of the rarest ions—C⁴⁻, Hf⁴⁺, I³⁺, In³⁺, Mo⁴⁺, S²⁺ and V²⁺—because all coexisting pairs that incorporate any of these ions are only known from one mineral. Links between nodes in our network models are based on the percentage occurrence of the rarer ion with the more common ion. Thus, ion pairs of the rarest ions will inevitably result in a high-percentage linkage that skews network topologies.

In Fig. 1, the node size indicates the number of occurrences of that ion in our tabulations of 4834 mineral species (Supplementary Table 1). Links between pairs of nodes indicate ion co-occurrence. Figure 1 illustrates the case where at least 18% of minerals incorporating the less common ion also incorporate the more common ion (based on percentages of ion co-occurrences tabulated in Supplementary Tables 1 and 3). Figure 1 is a static rendering of one state of the online dynamic interactive network in which several attributes of the network can be varied, including: (1) the minimum co-occurrence percentage, P, which can be varied from 1 to 70%; (2) the minimum number of minerals in Supplementary Table 1 with two co-occurring ions, which can be varied from 1 to 500; (3) the node size and the font size of node labels; and (4) the force constant of the force-directed network. Features also include the ability to exclude specific ions from the network and to recalculate distribution of ions among communities in real time as network parameters change. In addition, one can choose among four different community detection algorithms: Louvain, Informap, Label Propagation and Walktrap.

An important feature of Fig. 1 is the nonuniform distribution of ions among several communities that represent the most closely associated groups of ions. To determine the ion community structure in Fig. 1 we employed Louvain community detection analysis (Girvan and Newman, 2002; Fortunato, 2010), which is based on modularity optimisation (Blondel *et al.*, 2008). This method identifies members of a group in two steps: (1) form small communities, starting with each node as its own community, followed by maximising modularity of certain nodes; (2) aggregate each small community into 'super nodes' to form a new 'super node network'. These two steps are repeated until the network is optimised.

The Louvain modularity approach is unsupervised with respect to the number of resultant communities. Based on the network with $P \ge 18\%$ and excluding eight ions as noted above, we observe two principal communities of 31 and 23 mineral-forming ions, two smaller communities of 13 and eight ions, as well as two binary communities, each with two ions (Table 1). Each community represents a distinct suite of ions that commonly co-occur.

Community 1 (Louvain)

Thirty one orange-coloured ion nodes dominate the left half of Fig. 1 as a well-defined Community 1. These ions include several of the most common lithophile cations in igneous and metamorphic oxides and silicates—e.g. Al³⁺, Ca²⁺, Fe²⁺, K⁺, Mg²⁺, Na⁺ and

Si⁴⁺ found in feldspar, mica, pyroxene, amphibole, garnet and clay mineral groups, as well as many other rock-forming phases. Some of these common ions adopt central positions with high network centrality, which anchor an arcuate arrangement of other Community 1 nodes in the lower left. Community 1 features the defining ions of carbonates (C^{4+}) and phosphates (P^{5+}), as well as ions of primary minerals in complex pegmatites (B³⁺, Be²⁺, Cs⁺, F⁻, Li⁺, Rb⁺, Sc³⁺, Sn⁴⁺, Th⁴⁺, U⁴⁺; Černý, 1991; London, 2008), in carbonatites and/or agpaitic rocks (REE³⁺, Ce⁴⁺, Nb⁵⁺, Ti³⁺, Ti⁴⁺, Y³⁺, Zr⁴⁺; Mitchell, 1996a, 1996b; Marks and Markl, 2017), and in layered mafic intrusions (Cr3+; O'Driscoll and Van Tongeren, 2017). Note that Community 1 also includes most of the ions that are characteristic of stellar minerals (Hazen and Morrison, 2020) and the earliest nebular condensates found in chondrite meteorites (Morrison and Hazen, 2020). Most of the ions in Community 1 occur in only one oxidation state—exceptions being Cr, I, S, Ti, U and V. Notably absent from Community 1 ions are semi-metal chalcophile elements. As a result, the average electronegativity of 30 Community 1 cations is 1.45—the lowest of any community, while the only anion (F-) has the highest known electronegativity, 3.98. Consequently, the average bonding character among minerals with Community 1 ions, all of which contain O²⁻ and/or F⁻, tends to be more ionic than in the other communities.

Community 2 (Louvain)

The 23 red-coloured nodes in Fig. 1 are concentrated in a circular region of the upper half of Fig. 1. A halo of smaller nodes represents less common ions, most of which are connected to the centrally located nodes for relatively common Cu²⁺ and Pb²⁺. Community 2 is notable for hosting five of the eight anions in this study (Br-, Cl^- , I^- , N^{3-} and S^{2-}). The halogen anions are common constituents of hydrothermal brines and evaporite minerals (Guilbert and Park, 1986; Pirajno, 2009; Poot et al., 2024); whereas N³⁻ is found in 95 ammonium-bearing biominerals, many of which are associated with Phanerozoic urine, guano and plant decay (Hazen and Morrison, 2022). The sulfide anion, S^{2-} , occurs in 22 of the minerals recorded in Supplementary Table 1, all of which also incorporate O²⁻ and/or a halogen anion. Community 2 includes monovalent and divalent transition metal cations (Ag⁺, Cu⁺, Cu²⁺, Hg⁺ and Hg²⁺) typical of near-surface hydrothermal settings. Of special note are the close associations among Ag⁺, Cu⁺ and Hg⁺ with the halogens Br⁻, Cl⁻ and I⁻ (Dunning et al., 2005; Hazen et al., 2012). Of the remaining ions, ten are of metalloids (Ge, Sb and Te) or other cations with relatively high electronegativity (Pb, S, Se and Tl). Community 2 also hosts Cr⁶⁺, which is found in 26 chromate minerals, both as alteration phases via oxidation of other Cr-bearing minerals in soils, and as hydrothermal alteration products (Liu et al., 2017; Morrison et al., 2017, their figure 4). Additionally, Community 2 features the nitrate (N5+) ion, which invariably forms the $(N^{5+}O^{2-}_{3})$ -anionic group and is found in 20 minerals typically derived from urine or guano. Most of the Community 2 ions are relatively rare; 16 of the 23 ions are found in fewer than 30 of the 4834 minerals recorded in Supplementary Table 1. The average electronegativities of Community 2's 18 cations and five anions are 2.12 and 2.88, respectively—a substantially smaller difference than for Community 1, suggesting a comparatively more covalent average character. Of note is the strong discrimination between ions of Communities 1 and 2 in Fig. 1—a topology that suggests these two contrasting groups of ions do not frequently co-occur.

Community 3 (Louvain)

The 13 green nodes of Community 3, located in the centre-right of Fig. 1, include primarily ions of siderophile and chalcophile transition metals (Cd^{2+} , Co^{2+} , Co^{3+} , Mo^{5+} , Mo^{6+} , Ni^{2+} , V^{4+} , V^{5+} and Zn^{2+}). Note that this community has no anions; rather, this community links the anionic clusters $(As^{5+}O^{2-}_4)^{3-}$ and $(S^{6+}O^{2-}_4)^{2-}$ that are closely associated with hundreds of arsenate and sulfate minerals, most of which form through alteration/oxidation of primary chalcogenide deposits (Chang *et al.*, 1996; Hazen and Morrison, 2022). In this respect, Community 3 is more closely tied to (and partially overlaps with) Community 2 in Fig. 1. The average electronegativity of Community 3's 13 cations is 1.92, which is intermediate between those of Communities 1 and 2.

Community 4 (Louvain)

The eight blue nodes of Community 4 represent cations of two commonly associated first-row siderophile transition elements (Fe³⁺, Mn²⁺, Mn³⁺ and Mn⁴⁺), as well as the defining cations of antimonates (Sb⁵⁺), arsenites (As³⁺), tellurites (Te⁴⁺), and tungstates (W⁶⁺), all of which have fewer than 80 representative minerals. Community 4 nodes are anchored by the relatively common Fe³⁺ ion, which is linked to the seven other Community 4 cations, as well as to ions in Communities 1, 2 and 3. In particular, these ions are interspersed with those of Community 3; both groups of ions are most commonly associated with alteration/oxidation of primary chalcogenide minerals (Hazen and Morrison, 2022). The average electronegativity of Community 4 cations is 1.90, similar to that of Community 3.

Community 5 (Louvain)

Two ions, Sn^{2+} and Ta^{5+} , form their own Community 5 as a pair of brown nodes on the extreme bottom of Fig. 1—close to the nodes of Community 1, with which Ta^{5+} is also linked. These two ions are both relatively scarce in minerals, with six and 58 examples, respectively. Only two minerals, oxystannomicrolite ($Sn^{2+}_{2}Ta^{5+}_{2}O_{6}O$) and thoreaulite ($Sn^{2+}_{2}Ta^{5+}_{2}O_{6}$), contain both ions. However, because O^{2-} is the only other ion in these minerals, these two cations are particularly strongly linked (hence forming a separate community). However, these ions are also closely associated with Ca^{2+} , Mg^{2+} , Nb^{5+} and Y^{3+} —all cations in Community 1

Community 6 (Louvain)

The two ions of uranium with highest oxidation states, U^{5+} and U^{6+} , lie at the upper-left of Fig. 1, adjacent to several high field strength cations of both Community 1 and Community 2. These cations are associated with late-stage igneous fluids (e.g. with Ce^{4+} , Th^{4+} , Y^{3+} and REE^{3+}). U^{5+} occurs in only three minerals, but all three of those minerals also incorporate the more common U^{6+} , which occurs in 283 minerals. This 100% association of U^{5+} with U^{6+} is sufficient to create a separate community, even though U^{6+} is frequently found with Ca, K, Si and other lithophile cations of Community 1.

With 85 nodes representing mineral-forming ions (excluding $\rm H^+$ and $\rm O^{2-}$), the maximum number of ion pairs possible in Fig. 1 is $[(85^2-85)/2]=3570$ edges. In the case of mineral-forming ions, far fewer pairs are observed. The network 'density', D, is the fraction of the possible edges that are observed—a number that typically

decreases with increasing P. One conclusion of this study is that the great majority of possible ion pairs are not observed. For example, at P = 0% with all observed ion pairs represented by network edges, the network density is (1222/3570) = 0.342.

Results of Louvain community detection depend on the selection of network nodes as well as the percentage cutoff, P, for network edges. Therefore, we also performed Louvain community detection analysis for $P \geq 25$ and $P \geq 50\%$ (based on percentages recorded in Supplementary Table 3). At P=0%, the centre of the graph is occupied by Na⁺, Ca²⁺, Fe²⁺, Fe³⁺, Mg²⁺, Mn²⁺, Al³⁺, Si⁴⁺, P⁵⁺ and Ti⁴⁺, the majority of constituents needed to form most of the rocks in the Earth's crust. By removing these essential ions, the underlying trends of co-occurrences among less common ions become more evident, with patterns that are dependent on relatively restrictive paragenetic environments in which specific P-T-X conditions are met.

At $P \ge 20\%$, W⁶⁺ becomes the first of the 85 ions that is no longer connected to the network. At $P \ge 25\%$, 79 nodes remain (the cations Mo⁴⁺, Sb⁵⁺, Sn²⁺, Ta⁵⁺, W⁶⁺ and Zn²⁺ are no longer connected), with 190 of 3081 possible edges (D = 0.062). At $P \ge 50\%$, only 35 ion nodes remain connected to each other with a sparse 38 edges (out of 595 possibilities) between ion pairs (D = 0.064). It is intriguing that as nodes become disconnected with increasing P above 18%, the network becomes smaller but the density appears to remain relatively constant at ~0.06.

As P increases, and as ions and edges are consequently removed, the interactive graphics package (https://observablehq.com/d/726edcffdbc8fecc) automatically recalculates the community structure of the network. Therefore, the detailed distribution of ions among communities differs with P. Nevertheless, Community 1 always appears as the dominant feature, with strong connections among the most common mineral-forming ions, including Si^{4+} , Al^{3+} , Ca^{2+} and Na^+ .

Walktrap community detection

We applied multiple methods for community detection to the ion co-occurrence data. In contrast to Louvain community detection, which is based on modularity optimisation, the Walktrap algorithm analyses connections among nodes based on the lengths of random walks. The Walktrap algorithm assumes that random walks tend to spend more time within the same community due to the denser internal connections within that community (Pons and Latapy, 2005). In detail, the Walktrap algorithm clusters communities by simulating multiple random walks, calculating their path similarities, and then merging nodes using hierarchical clustering. Due to the nature of random walks, community detection in Walktrap is influenced by local relationships, leading to the formation of closely connected communities.

Though both Louvain and Walktrap algorithms aim to optimise community structure, they differ in their approaches. The Louvain algorithm follows a bottom-up greedy strategy, initially treating each node as an individual community and iteratively merging them to maximise modularity (Blondel *et al.*, 2008). With its nearly linear time complexity, the Louvain algorithm is highly efficient for processing large-scale networks. In contrast, the Walktrap algorithm is better suited for capturing finer local community structures.

Figure 2 is a unipartite network with initial parameters P = 20%. The two most common ions (H⁺ and O²⁻) and seven of the least connected rare ions (C⁴⁻, Hf⁴⁺, I³⁺, In³⁺, Mo⁴⁺, S²⁺, V²⁺ and W⁶⁺) are excluded from the network, leaving 78 nodes. In Fig. 2

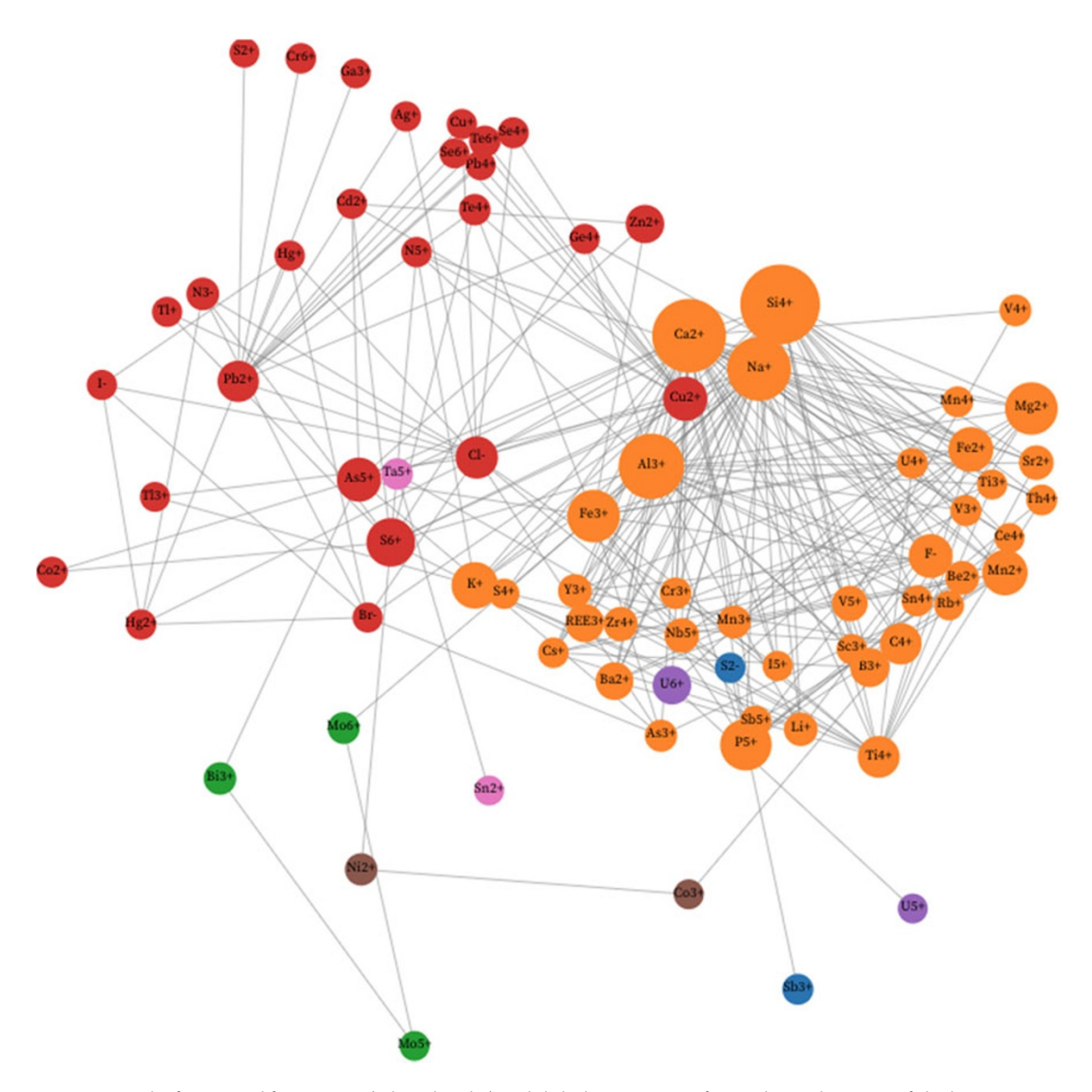


Figure 2. A unipartite network of 78 mineral-forming ions (coloured circles), with links between pairs of ions when at least 20% of the less common ion also occurs with the more common ion. Node sizes indicate the relative abundances of ions, while colours indicate communities determined using the Walktrap method (see text). The resulting analysis reveals two major communities of 40 and 27 nodes representing mineral-forming ions plus five minor communities, each with two or three nodes. Each of the two larger communities corresponds to groups of ions that co-occur relatively frequently. The 40 orange nodes of Community 1 include all 31 Community 1 ions from Fig. 1. Community 2 includes 27 ions represented by red nodes, 21 of which also correspond to Community 2 in Fig. 1. This figure is a static Image of an Interactive web-based graphic (see https://observablehq.com/d/726edcffdbc8fecc).

we employed the Walktrap algorithm instead of Louvain community detection (see https://observablehq.com/d/726edcffdbc8fecc). Figure 2 displays many of the same features as Fig. 1. Both networks display two dominant communities that are significantly separated from each other, as recorded in Table 1.

Community 1 (Walktrap)

The 40 orange-coloured nodes that populate the righthand side of Fig. 2 include all 31 ions of Louvain Community 1 in Fig. 1, as well as I^{5+} from Louvain Community 2; As^{3+} , V^{4+} and V^{5+} from Louvain Community 3; and Fe^{3+} , Mn^{2+} , Mn^{3+} , Mn^{4+} and Sb^{5+} from Louvain Community 4. As in Fig. 1, the most common lithophile ions (Al^{3+} , Ca^{2+} , K^+ , Na^+ and Si^{4+}) assume central positions, in this case connected to an arc of less common ions to the lower right.

Community 2 (Walktrap)

Community 2 links 27 red-coloured nodes, of which 21 are also in Louvain Community 2 of Fig. 1. The other six ions in the Walktrap version of Community 2 are Co^{2+} , S^{6+} , Tl^+ and Zn^{2+} , which are in Louvain Community 3, and As^{5+} and Te^{4+} in Louvain Community 4. As in Fig. 1, the separation of Walktrap Communities 1 and 2 is striking.

Community 3 (Walktrap)

Three green nodes representing $\mathrm{Bi^{3+}}$, $\mathrm{Mo^{5+}}$ and $\mathrm{Mo^{6+}}$, form a separate Walktrap community at the bottom left. These ions, all of which are found in Louvain Community 3 of Fig. 1, are closely associated because $\mathrm{Mo^{5+}}$ occurs in only three minerals,

two of which also incorporate the more common Bi^{3+} {gelosaite $[Bi^{3+}Mo^{6+}_{(2-5x)}Mo^{5+}_{6x}O_7(OH)\cdot H_2O\ (0\leq x\leq 0.4)]$ and mambertiite $[Bi^{3+}Mo^{5+}_{2.80}O_8(OH)]$ }, while two incorporate Mo^{6+} {gelosaite and novikovite $[(N^{3-}H_4)_4Mo^{6+}_2Mo^{5+}_2O_8(S^{6+}O_4)_5]$ }.

Community 4 (Walktrap)

Two blue nodes in Fig. 2 represent S^{2-} and Sb^{3+} —a community that reflects the co-occurrence of these ions in six of the 22 rare S^{2-} minerals recorded in Supplementary Table 1. Both ions occur in Louvain Community 2 in Fig. 1.

Community 5 (Walktrap)

Two brown nodes connect the transition metal ions Co^{3+} and Ni^{2+} . These two siderophile ions are closely linked because four of the six Co^{3+} minerals recorded in Supplementary Table 1 also contain Ni^{2+} . These two ions occur in Louvain Community 3 in Fig. 1.

Community 6 (Walktrap)

The two purple ions of Walktrap Community 6 (U^{5+} and U^{6+}) are the same as Community 6 determined by Louvain community detection in Fig. 1. As noted above, all three U^{5+} minerals in Supplementary Table 1 also contain U^{6+} , thus creating a strong association.

Community 7 (Walktrap)

Community 7, which holds two nodes representing Sn²⁺ and Ta⁵⁺, is identical to Louvain Community 5 in Fig. 1.

Comparisons between Fig. 1 based on Louvain community detection and Fig. 2 based on the Walktrap algorithm reveal many small differences, but significant overall similarities in the network structures. In particular, in both approaches most mineral-forming ions separate into two large communities, one of which (Community 1 in both cases) includes ions of most lithophile elements found in common rock-forming igneous and metamorphic rocks, whereas the other (Community 2 in both Figs 1 and 2) includes primarily ions of chalcophile elements found in minerals associated with near-surface processes of weathering, oxidation, aqueous alteration and evaporation.

Of the smaller communities, nine of 13 ions in Louvain Community 3 match ions distributed among Walktrap Communities 2, 3 and 5, while five of eight Louvain Community 4 ions are located in Walktrap Community 1. These distributions underscore similarities in the visual distributions of ion nodes in Figs 1 and 2. In both networks, Communities 1 and 2 are well separated, whereas ions of smaller communities display greater overlaps with adjacent communities.

Heatmap and agglomerative hierarchical cluster analysis of co-occurring ions

Heatmaps coupled with hierarchical cluster analysis provide a complementary approach to visualising patterns of co-occurrence among mineral-forming ions (Fig. 3). Building upon the mineral data heatmap visualisation demonstrated by Que *et al.* (2024) and Zhang *et al.* (2024), we utilised the *Plotly* Package of Python (Plotly Technologies Inc., 2015) and determined the sequence of ions with agglomerative hierarchical clustering (Maimon and Rokach, 2006).

We applied the 87×87 diagonally symmetric data matrix that lists percentages of co-occurrences between pairs of mineralforming ions (see Supplementary Table 3) to the heatmaply function. This method performed agglomerative hierarchical clustering with a complete linkage approach to map ions in the heatmap so that ions with higher percentages of co-occurrences are placed closer to one another. Thus, for example, the two most commonly co-occurring ions, O2- and H+, are grouped next to each other and form the bottom two rows and two lefthand columns of the matrix. Similarly, U⁵⁺ appears adjacent to U⁶⁺ because all three U⁵⁺ minerals also contain U⁶⁺. Each matrix element represents the co-occurrence of two ions, with more intense colours indicating higher percentages of co-occurrence. Figure 3 thus provides both an alternative approach to visualising the most strongly associated ions, while having the valuable ability to highlight ion antipathies those systematic absences of large groups of ion pairs in the mineral kingdom, as indicated by regions AB, AD, AE and BE. In this way, heatmap analysis is complementary to the network visualisation and community detection algorithms applied to ion co-occurrence data in Figs 1 and 2.

A particularly useful aspect of hierarchical cluster analysis is the 'tree diagram' that appears on both the bottom and, equivalently, on the lefthand side of Fig. 3. This branching representation reveals pairs, triads, and larger clusters of ions that most frequently cooccur. Accordingly, one can select any desired number of clusters, from merging all ions into a single global cluster of 87 ions, to 87 individual clusters, each of which is a different ion. To compare this approach to the unipartite networks of Figs 1 and 2, we identified and examined seven major clusters of minerals arranged along the diagonal axis and designated Clusters A to G (Table 1), with $\rm O^{2-}$ and $\rm H^+$ forming an eighth cluster of only two strongly associated ions.

Comparisons between Network Communities and Heatmap Clusters

The minerals in each Cluster A to G, and their correspondences to Louvain Communities 1 to 6 in Fig. 1 and Walktrap Communities 1 to 7 in Fig. 2, are identified in Table 1. As might be expected, significant similarities emerge, while there are also important differences.

Cluster A

The upper righthand area of Fig. 3 features a cluster of 13 ions, most of which are scarce and only one of which is an anion (N^{3-}). Most of the ions are siderophile or chalcophile transition metals and semi-metals (As^{5+} , Bi^{3+} , Co^{2+} , Co^{3+} , Ga^{3+} , Ge^{4+} , In^{3+} , Ni^{2+} , Tl^+ , V^{4+} and V^{5+}). Of these ions, 11 come from Louvain Communities 2 and 3 in the upper right of Fig. 1 or, equivalently, Walktrap Communities 2, 3, and 5 from the left side of Fig. 2. This arrangement provides additional support for the close association of Louvain Communities 2 and 3.

Cluster B

Cluster B, with 23 ions, is the largest cluster in Fig. 3. Of those ions, 15 are also in Louvain Community 1, while an additional six are in Louvain Community 4—a distribution of 21 ions that underscores the close association between Louvain Communities 1 and 4 in Fig. 1. Indeed, those same 21 ions are all in Walktrap Community

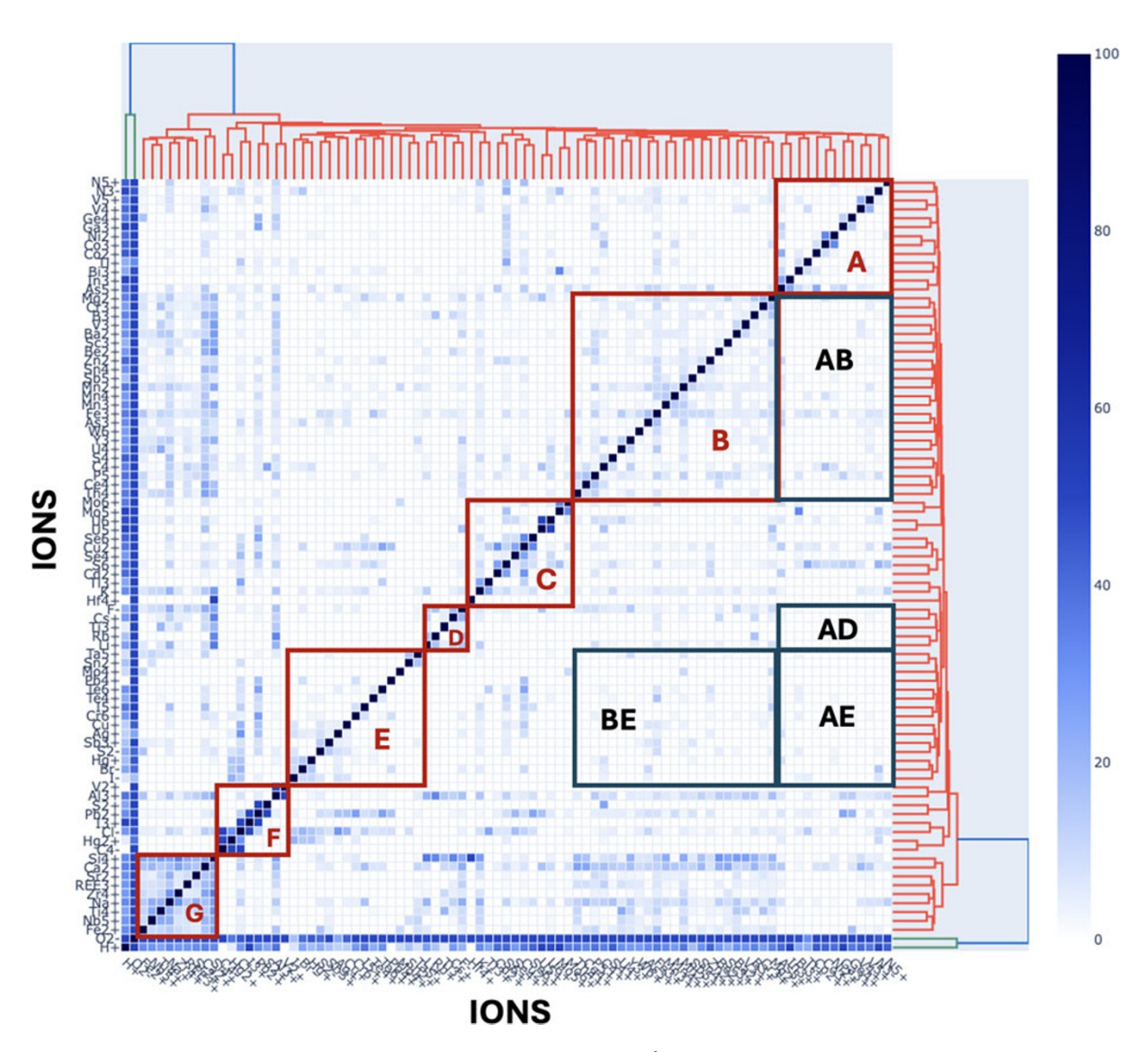


Figure 3. This 87×87 heatmap (in this case including the two most common ions, H^+ and O^{2-}) displays a diagonally symmetrical matrix of coexisting mineral-forming ions, with 3741 unique non-diagonal matrix elements. Each matrix element represents the percentage of the rarer ion that coexists with the more common ion (Supplementary Table 3) in a list of 4834 minerals (Supplementary Table 1; see text), as defined by the colour scale. Ions that co-occur most frequently are indicated by darker coloured matrix elements. The order of ions from both top to bottom and from right to left was determined by agglomerative hierarchical clustering using the heatmaply package of R (Galili et al., 2018), which grouped ions according to their most frequent associations. Adjacent pairs of ions are most closely related, with larger groups arranged hierarchically, as indicated by the hierarchical tree on the top (and, equivalently, the righthand side) of the matrix. We highlight seven clusters, labelled A to G, as well as four sparsely-populated regions labelled AB, AD, AE and BE (see text).

1 in Fig. 2. Of the 21 different elements represented in Cluster B, 13 are lithophiles according to Goldschmidt classification.

Cluster C

The 12 cations of Cluster C are predominantly from Louvain and Walktrap Communities 2 and 3, occurring in the upper right of Fig. 1 and the left side of Fig. 2. Seven of these 12 ions are high field strength cations (Hf^{4+} , Mo^{5+} , Mo^{6+} , Se^{4+} , Se^{6+} , U^{5+} and U^{6+}).

Cluster D

Cluster D features only five ions (Cs⁺, F⁻, Li⁺, Rb⁺ and Ti³⁺), all of which are ions of lithophile elements that occur in Community 1 of both Figs 1 and 2.

Cluster E

Most of Cluster E's 15 ions (Ag⁺, Br⁻, Cr⁶⁺, Cu⁺, Hg⁺, I⁻, I⁵⁺, Mo⁴⁺, Pb⁴⁺, S²⁻, Sb³⁺, Sn⁴⁺, Ta⁵⁺, Te⁴⁺ and Te⁶⁺) are relatively uncommon constituents of near-surface alteration and aqueous processes (Hazen and Morrison, 2022). These ions, mostly of chalcophile elements, are closely associated with Louvain Communities 2 and 5 (13 of 15 ions) and Walktrap Communities 2, 4 and 7 (the same 13 of 15 ions).

Cluster F

The eight ions of Cluster F include an eclectic mix of relatively common ions from Louvain/Walktrap Communities 1 (Al^{3+}) and 2 (Cl^- , Hg^{2+} and Pb^{2+}), as well as some of the rarest ions— S^{2+} is recorded from two minerals in Supplementary Table 1, whereas

 $C^{4^{-}}$, I^{3+} , and V^{2+} are recorded from only one mineral. Indeed, the latter three ions have been excluded from the networks of Figs 1 and 2. Aluminium joins this cluster because the only V^{2+} mineral is a vanadium aluminate, dellagiustaite $[V^{2+}Al_2O_4]$, which results in a 100% association of V^{2+} with Al^{3+} . Similarly, the only I^{3+} mineral, schwartzembergite $[Pb^{2+}{}_5H_2I^{3+}O_6Cl_3]$ has Pb^{2+} and Cl^- (Welch $\it et al., 2001$), whereas the only C^{4-} mineral, mikecoxite $[(C^{4-}Hg^{2+}{}_4)OCl_2]$, has Hg^{2+} and Cl^- (Cooper $\it et al., 2023$). In the case of S^{2+} , known only in boojumite $[Pb^{2+}{}_8O_4(OH)_2(S^{2+}{}_2O_3)^{2-}{}_3]$ and fassinaite $[Pb^{2+}{}_2(CO_3)(S^{2+}{}_2O_3)^{2-}]$, both minerals also incorporate Pb^{2+} . These 100% associations with the rarest ions illustrate how agglomerative cluster distributions may be distorted by mineral idiosyncrasies.

Cluster G

Cluster G, with nine cations (Ca²⁺, Fe²⁺, Na⁺, Nb⁵⁺, REE³⁺, Si⁴⁺, Sr²⁺, Ti⁴⁺ and Zr⁴⁺), includes several of the most abundant mineral-forming ions that occur in primary oxide and silicate minerals from igneous and metamorphic rocks (Hazen and Morrison, 2022; Hazen *et al.*, 2023a; Morrison *et al.*, 2024). All these cations occur in both the Louvain and Walktrap Communities 1 of Figs 1 and 2. This result demonstrates that the strong associations among these ions are independent of the community/cluster detection method employed.

The patterns observed with agglomerative clustering underscore that the different community/cluster detection methods employed in this study lead to similar (though in detail not identical) distributions of ions among two major groups, with important subgroups. The most obvious clusters of ions, shared by Figs 1, 2 and 3, feature the most common cations in igneous rocks, high field strength cations in oxidised ore zones, and ions associated with hydrothermal and near-surface brines. At the same time, 29 (33.3%) of the 87 mineral-forming ions occur in 20 or fewer minerals; consequently, patterns of their co-occurrence may be skewed by rare-ion distributions in ways that do not easily fall into welldefined communities or clusters. Consequently, the co-occurrence of a rare ion with more common ions often overrides geochemical association trends in arranging ions by these community detection and agglomerative clustering methods. Nevertheless, most clusters in Fig. 3 have strong overlaps with a single community in Figs 1 and 2. This result highlights the strong geochemical and paragenetic affinities that cause some groups of ions to seldom co-occur with other groups.

Missing ions and ion pairs

Our list of 87 mineral-forming ions represents fewer than half of all the known oxidation states of elements studied and identified in chemistry (Emsley, 1991; Greenwood and Earnshaw, 1997). We suggest two principal underlying reasons for these 'missing' mineralogical ions, as well as their ion pairs.

Missing ions

A principal reason for the absence of an ion in our tabulations is element rarity. The number of observed minerals for each essential chemical element is a function of that element's crustal abundances (Christy, 2015; Hazen *et al.*, 2015) and is consequently also closely tied to mineral rarity (Hazen and Ausubel, 2016; Gavryliv *et al.*,

2022). In many instances, ions of relatively rare elements have not yet been found as essential elements in any oxygen-based minerals. Notable examples are well-documented ions of siderophile noble metals (Au⁺, Au³⁺, Ir⁴⁺, Os²⁺, Os³⁺, Os⁴⁺, Pt²⁺, Pt⁴⁺, Re⁴⁺, Re⁷⁺, Rh³⁺, Ru³⁺ and Ru⁴⁺), which are all known in synthetic oxide phases, yet rarely bond with oxygen in terrestrial settings.

In addition, many ions, including a few of relatively common elements, are not found as essential constituents of minerals because they require either extremely reducing environments (Cr²⁺, Ga⁺, Ge²⁺, Nb²⁺, Nb⁴⁺, P³⁺, Ta⁴⁺, Ti²⁺ and W⁴⁺) or unusually oxidised conditions (Ag³⁺, Bi⁵⁺, I⁷⁺, Ni³⁺ and Pd⁴⁺). In some instances, as in polydymite [Ni²⁺Ni³⁺₂S₄] and siegenite [Co²⁺Ni³⁺₂S₄], these ions occur in chalcogenide minerals and probably await discovery in secondary oxide minerals. For example, synthetic Ni³⁺ compounds such as the oxide (Ni³⁺₂O²⁻₃; Aggarwal and Goswami 1961) and other compounds (e.g. Y³⁺Sr²⁺₅Ni³⁺₃O²⁻₁₁; James and Attfield, 1993), point to the possibility of as yet undocumented Ni³⁺–O²⁻ minerals. A similar case can be made for Ag³⁺–O²⁻ minerals: the synthetic reagents Ag³⁺₂O²⁻₃ and Ag²⁺Ag³⁺₂O²⁻₄ (Greenwood and Earnshaw, 1997) are well known mineral-like compounds that might be formed in extremely oxidising, silver-rich terrestrial environments.

In at least three examples, such missing ions are known to exist as minor constituents of rock-forming minerals, but they are not yet known to occur in sufficient concentrations to form their own mineral species. For example, the reduced Cr²⁺ ion, well known to chemists in the reagent chromium monoxide (Cr²⁺O²⁻), has been documented by spectroscopic evidence as a minor constituent of lunar olivine (Hazen et al., 1977), though it is not yet known as an essential mineral-forming ion in oxides. Eu²⁺ is another wellknown example of a reduced ion occurring only as a trace element. The fractionation of minor amounts of Eu²⁺ and Eu³⁺ between feldspar and magmatic liquids leads to the so-called 'europium anomaly' in patterns of rare earth element distributions (Weill and Drake, 1973). Furthermore, the combination of the reducing conditions required and low concentrations of Eu in crustal rocks results in a low likelihood of Eu²⁺ minerals. In magmas [Eu³⁺/(total Eu)] ranges from 50% at the Iron-Wüstite buffer to 90% at Quartz-Fayalite-Magnetite (QFM) buffered rocks. Most magmas are at QFM or higher fO_2 , with $< 10\% \text{ Eu}^{2+}$ (Burnham et al., 2015). Other interesting cases are Nb and Ta, which only occur as pentavalent cations in our tabulations of oxide and halide minerals, yet are also known as trace divalent and tetravalent species in minerals (Martin and Wüsler, 2014, and references therein).

In a similar situation, the rarity of some mineral-forming ions in IMA-approved chemical formulas is often a consequence of masking by much more common ion of similar radius and valence. Thus Rb^+ is commonly masked by $K^+,\,Ga^{3+}$ by $Al^{3+},\,$ and V^{4+} by $Ti^{4+}.$ These and many other rare ions are commonly present in minerals, yet rarely appear in their chemical formulas.

These examples highlight a significant geochemical limitation of our dataset: we analysed only IMA-approved species-defining 'essential' ions in 4834 minerals. Consequently, significant information about the geochemistry of minor and trace elements and their oxidation states has been excluded from the list. Furthermore, the associations of ions change dramatically as a function of element concentrations. At trace levels, a variety of different substitution mechanisms or incorporation of ions in different structural defects is possible, however there is an upper limit to the incorporated trace element concentration possible with these mechanisms.

Even so, numerous minerals incorporate 100s to 1000s of ppm of relatively rare elements, though no IMA-approved formula with that element is known.

The expansion of mineral definitions and descriptions to include trace elements, ions, and isotopes is an important objective of mineral informatics. Further quantification of the distribution of trace ions among minerals would significantly expand the 87 ion list of this study. Such added data would also significantly affect the structure of the networks in Figs 1 and 2, both because different oxidation states of the same element can often have different geochemical affinities despite co-occurring in the same mineral species and because a given ion can occur in a much wider range of minerals at trace levels than as a minor or major constituent.

Ion antipathies and 'missing' ion pairs

Figure 3 reveals several largely blank, off-diagonal regions that represent groups of ions that rarely co-occur. These patterns of 'ion antipathies' [borrowing a term from Bowen (1928)] suggest systematic strong avoidances among many groups of mineral-forming ions. A question arises: are these systematic trends the result of crystal chemical constraints (i.e. ions that can never occur together because of structural/bonding limitations), or rather do they arise from the idiosyncrasies of geochemical sorting of elements and their ions?

To address this question we consider four particularly 'vacant' areas, or 'anticlusters', of Fig. 3, designated AB, AD, AE and BE. Recall that 1392 (37.2%) of 3741 possible co-occurring ion pairs are observed in at least one mineral species. Therefore, any region of Fig. 3 with significantly less than 37% occupancy represents an area of statistically significant ion antipathies.

Anticluster AB

The area labelled AB in Fig. 3, representing the 13 ions of Cluster A versus the 23 ions of Cluster B, is a relatively sparse region of the heatmap, as only 43 of 299 possible ion pairs (14.4%) have non-zero values. Most of these absences reflect the geochemical antipathies between the ions of both Louvain and Walktrap Communities 1 (represented by almost all ions in Cluster B) and Communities 2 (represented by Cluster A).

Anticluster AD

A similar situation pertains to a second markedly sparse area of Fig. 2 that is formed by pairs of the 13 ions in Cluster A versus the five ions in Cluster D, all of which occur in Louvain and Walktrap Community 1. Most of the Cluster D ions (Cs $^+$, F $^-$, Li $^+$ and Rb $^+$) are commonly associated with late-stage igneous fluids and rarely if ever associate with the transition elements and high field strength semimetals of Cluster A. Of the $5 \times 13 = 65$ possible pairs, only five (7.7%) have non-zero values, and none of the observed pairs has greater than 4% co-occurrence.

Anticluster AE

The sparse area of Fig. 3 represented by the 13 ions of Cluster A versus 15 ions of Cluster E presents a different situation. Both clusters include ions that are predominantly from Louvain Communities 2 and 3 and Walktrap Community 2 in Figs 1 and 2. Accordingly, one might expect significant co-occurrences among these ions. However, of the 195 possible ion pairs, only 21 pairs (10.8%)

have non-zero values. This significant absence of coexisting ion pairs within the well-defined Community 2 reveals that there are important substructures within this community. The Louvain and Walktrap algorithms identify communities in different ways, but both methods will lump ions that do not themselves co-occur if they are commonly connected through a third shared node. Thus, for example, while Community 2 ions Ga^{3+} and Ge^{4+} never co-occur in minerals with Pb^{4+} or Te^{4+} , all four ions are connected through Pb^{2+} .

Anticluster BE

A fourth poorly populated region of the heatmap occurs for Cluster B versus Cluster E—a 23×15 section in which only 52 (15.1%) of 345 possible ion pairs are nonzero. This situation is of special interest because Cluster B incorporates 11 relatively common mineral-forming ions, including B³⁺, Ba²⁺, Be²⁺, C⁴⁺, Cr³⁺, Fe³⁺, Mg²⁺, Mn⁴⁺, P⁵⁺, Sr²⁺ and Zr⁴⁺, all represented by more than 100 mineral species in Supplementary Table 1. Admittedly, most of the Cluster E ions are rare, with the exceptions of Cr⁶⁺, Sb³⁺, Sn²⁺, Ta⁵⁺, Te⁴⁺ and Te⁶⁺ (recorded in 61, 39, 41, 58, 54 and 52 mineral species, respectively). None of the other Cluster E ions occurs in more than 19 minerals. Nevertheless, we find that no known minerals combine pairs of relatively common ions, such as Be^{2+} , Cr^{3+} , or Sr^{2+} with Sb^{3+} , Ta^{5+} , Te^{4+} , or Te^{6+} . Similarly, Zr^{4+} does not co-occur with Sb^{3+} , Te^{4+} , or Te^{6+} ; neither does Mg^{2+} co-occur with Sb³⁺; and the pairs Mg²⁺/Ta⁵⁺ and Zr⁴⁺/Ta⁵⁺ are each known from only one mineral species. We suggest that these absent or rare ion pairs reflect geochemical rather than crystal chemical constraints. For example, the Crystallography Open Database (https:// www.crystallography.net/cod/search.html, accessed 24 December 2024) lists two synthetic inorganic oxide phases with Be²⁺ and Te⁶⁺; 30 phases with Mg²⁺ and Ta⁵⁺; 34 phases with Cr³⁺ and Sb³⁺ or Sb⁵⁺; and 37 phases with Sr²⁺ and Te⁴⁺ or Te⁶⁺.

A conclusion from these observations of ion antipathies is that the list of co-occurring ion pairs in minerals reflects limitations in the chemical compositions of mineral-forming fluids and the idiosyncrasies of near-surface paragenetic modes, more than crystal chemical restrictions. For example, ions in Cluster D that are commonly associated with late-stage igneous fluids (Cs⁺, F⁻, Li⁺ and Rb⁺) rarely if ever associate with Cluster E's low field strength ions found concentrated in brines (Ag⁺, Br⁻, Cu⁺, Hg⁺ and I⁻) or with high field strength ions from weathered primary oxide or sulfide deposits (Cr⁶⁺, Pb⁴⁺, Mo⁴⁺, Te⁴⁺ and Te⁶⁺).

Note, however, that such combinations of ions are not precluded on strictly crystal chemical grounds, as evidenced by such synthetic compounds as BTe₃O₃F₁₅ (Sawyer and Schrobilgen, 1982), RbMo₂P₃O₁₂ (Leclaire and Raveau, 1988), LiAg₂N₃O₆ (Ishihara et al., 1986), CdCs₂I₄ (Touchard et al., 1987), and scores of other examples recorded in the Crystallography Open Database (see https://www.crystallography.net/cod/result.php, accessed 24 December 2024). Mineral occurrences depend on their P-T-X conditions of formation. For example, the formation of a mineral such as BTe₃O₃F₁₅ requires relatively high oxygen and fluorine fugacities, in addition to high activity of B-conditions that are geochemically unrealistic. Furthermore, in most natural environments if Te is sufficiently concentrated it will form a telluride or will be incorporated into a chalcogenide mineral. We conclude that the absence of such synthetic compounds in the mineral realm, and the corresponding 'missing' ion pairs, is a consequence of geochemical, not crystal chemical, restrictions.

Conclusions

Our analysis of 87 co-occurring ions in 4834 minerals with oxygen and/or halide anions reveals that 1392 different pairs of ions (out of 3741 possible combinations) coexist in minerals. Employing varied methods of community detection and agglomerative clustering, we demonstrate that both element abundances and geochemical affinities among elements in mineral-forming environments play key roles. A key finding is that the majority of these ions fall in one of two contrasting communities/clusters—one corresponding to the most common ions in rock-forming igneous and metamorphic rocks, and the other with ions primarily found in near-surface zones of weathering, oxidation, aqueous alteration and evaporation. Most ions in Community 1 rarely, if ever, co-occur with ions in Community 2.

Why do many ions never co-occur?

Detailed analysis of all 2349 pairs of ions that are not observed—more than 60% of the 4834 possible combinations in Supplementary Table 1—is beyond the scope of this contribution. However, it is evident that most missing ion pairs arise primarily because of a combination of three factors: (1) the rarity of many elements and therefore the statistical improbability of many pairs to occur in high enough concentration/activity to be an essential constituent of a mineral phase rather than just a trace to minor element; (2) geochemical antipathies among ions, for example of contrasting oxidation states; and (3) the idiosyncrasies of many mineral-forming environments, rather than any systematic crystal chemical limitations.

As we have seen, in many cases geochemical processes tend to separate disparate groups of elements: the most abundant elements in the late-stage fluids that form complex pegmatites differ from elements in sulfide-rich melts or halogen-rich brines. Indeed, many of the 'nonintuitive' chemical combinations represented by the extensive areas of rare to nonexistent ion pairs might point to fruitful grounds for future synthetic chemical exploration. Large compilations of the structures and properties of synthetic inorganic compounds (e.g. https://www.crystallography. net/cod/result.php and https://icsd.fiz-karlsruhe.de/search/basic. xhtml, accessed 24 December 2024) reveal that many of the ion combinations not observed in minerals are readily incorporated into synthetics. However, it is important to note that geochemical and crystal chemical conditions are sometimes intertwined. The fact that two ions coexist in synthetic compounds, but are not found together in any known mineral may be in some cases a consequence of high bonding energies requiring special synthesis conditions not likely to occur naturally.

In other instances, two elements may commonly co-occur yet their ions of extreme oxidation states cannot. For example, Mn and Ti co-occur in 62 minerals, Mn and V co-occur in 32 minerals, U and V co-occur in 22 minerals, and Ti and U co-occur in 18 minerals (https://rruff.info/ima; accessed 15 February 2025), yet the relatively oxidised cations Mn⁴⁺ or U⁶⁺ are unlikely to co-occur with reduced ions such as Ti³⁺ or V²⁺ in any stable phase.

The roles of electronegativity and paragenetic modes

The groupings of ions, such as those illustrated in Figs 1, 2 and 3, have been highly influenced by evolving near-surface redox environments, which have changed systematically and significantly through Earth history (Hazen *et al.*, 2008, 2023b; Hazen and

Morrison, 2022; Zhuang et al., 2024). Of note, Moore et al. (2022) documented systematic changes in average electronegativity of minerals through Earth history—changes that reflect how the range of redox conditions on Earth's surface have expanded significantly over the past 4 billion years, while greatly increasing Earth's mineral diversity and chemical complexity (e.g. Hazen et al., 2008; Krivovichev et al., 2022; Moore et al., 2024a; 2024b). The mineral evolution of several redox-sensitive elements, including uranium (Hazen et al., 2009), mercury (Hazen et al., 2012), carbon (Hazen et al., 2013), chromium (Liu et al., 2017), and vanadium (Liu et al., 2018) demonstrate details of the systematic increases in the average oxidation state of those elements, and thus the possibilities of new co-occurring ion pairs, especially since the Great Oxidation Event of the Paleoproterozoic Era (Hazen, 2015).

Our study also suggests that changes in mineral-forming conditions on Earth have led to the expansion and emergence of new communities of mineral-forming ions in conjunction with new paragenetic modes. Earth's earliest mineral-forming ions occur predominantly in the primary igneous minerals, and subsequently metamorphic minerals, reflected in Community 1 of this study. Subsequent introduction of new near-surface paragenetic modes are reflected in Community 2, which is dominated by co-occurring ions in minerals formed by near-surface processes since the Great Oxidation Event. Future studies will examine the chronological appearance of new mineral-forming ions, based on the sequence of new paragenetic modes (Hazen and Morrison, 2022; Hazen et al., 2023b). This effort will rely on the capabilities of graph theory and community detection analyses to visualise complex datasets influenced by several variables such as redox states, P-T-Xconditions, time and other geochemical and crystal chemical constraints.

Goldschmidt's classification revisited

This study demonstrates the ongoing relevance of Goldschmidt geochemical classification of the elements (Goldschmidt, 1923, 1937, 1954), while suggesting an important modification. The division of mineral-forming elements into siderophile, chalcophile and lithophile groups is a valuable framing of the periodic table in the context of planetary evolution. In one sense, our study of the distribution of mineral-forming ions underscores this division, as the ions of most elements in this study appear to separate into two main groups—the predominantly lithophile elements of Community 1 and the chalcophile elements of Community 2. We find that of the 31 ions in Louvain Community 1, 27 are Goldschmidt lithophile elements. By contrast, 16 of 23 ions in Louvain Community 2 are chalcophile. The community/cluster structure of Figs 1, 2 and 3 are thus in large measure a reflection of contrasting element types. Furthermore, only six of Goldschmidt's 14 siderophile elements (Mn, Fe, Co, Ni, Mo and W) are represented by our studies of oxygen- and/or halide-bearing minerals.

However, discrepancies appear when different oxidation states of an element are considered. For example, in both Louvain and Walktrap analyses, the lithophile element chromium appears in Community 1 in its Cr^{3+} state, but in Community 2 in the more oxidised Cr^{6+} state. Similarly, As^{3+} occurs in Walktrap Community 1, but As^{5+} is in Walktrap Community 2. The abundant ions Fe^{2+} and Fe^{3+} fall in Louvain Communities 1 and 4, respectively; Sb^{3+} and Sb^{5+} occur in Louvain Communities 2 and 4, respectively; and the different ions of thallium, tin, uranium and vanadium also span two different Louvain and Walktrap communities.

Goldschmidt recognised this aspect of elements with variable oxidation states. For example, he states: "chromium is a strongly lithophile element under ordinary terrestrial conditions. If, however, oxygen is deficient, as in iron meteorites, chromium is decidedly chalcophile, entering almost exclusively into the sulpho-spinel daubréelite, $FeCr_2S_4$ " (Goldschmidt, 1937; p. 659). Similarly, iron is a siderophile element, preferentially found in the metallic state in planetary cores. However, in its Fe^{2+} state iron often behaves as a chalcophile, while Fe^{3+} is usually bonded to oxygen as a lithophile element. In general, the more oxidised the ion, the more lithophile is its character.

Our study suggests an intriguing wrinkle in this trend. Here we consider the subset of minerals with cations bonded to ${\rm O^{2-}}$ and/or halogen anions. Therefore, by definition, we are limiting our analysis to lithophile contexts, albeit with the participation of many ions of chalcophile or siderophile character in the Goldschmidt sense. At a planetary scale, the more oxidised state of an element is typically more lithophile in character—a significantly greater fraction of ${\rm As^{5+}}$, ${\rm Cr^{6+}}$, and ${\rm Fe^{3+}}$ minerals are bonded to ${\rm O^{2-}}$ than ${\rm As^{3+}}$, ${\rm Cr^{3+}}$, or ${\rm Fe^{2+}}$ minerals, which frequently form chalcogenide minerals. This tendency has been formalised by Christy (2018a, 2018b), who derived energetic parameters that distinguish among siderophile, chalcophile, 'soft lithophile' (e.g. large-ion lithophiles), and 'hard lithophiles' (high field strength elements).

Nevertheless, in this study, we find that ions in their lower oxidation states, such As³⁺, Cr³⁺ and Fe²⁺, are typically grouped with the unambiguously lithophile elements of Community 1, including Al, Ba, Be, Ca, K, Li, Mg, Na, P, REE, Rb, Si, Ti and Zr. By contrast, the more oxidised As⁵⁺, Cr⁶⁺ and Fe³⁺ ions fall into Community 2, where they are most strongly linked to chalcophile elements, including Ag, Cu, Ga, Ge, Hg, Pb, Sb, Sn, Te and Zn. This unanticipated result reflects the fundamental role of evolving paragenetic modes in the distribution of mineral-forming elements.

At the time of planetary formation, siderophile elements preferentially concentrated in the dense metal fraction that would become Earth's core. The contrasting relatively low densities of many oxides and silicates concentrated lithophile elements in the crust and chalcophile elements initially formed primarily sulfides, arsenides and other chalcogenide minerals of intermediate average density. Subsequent tectonic processes led to new volcanic and metamorphic mechanisms that concentrated chalcophile and, to a lesser extent, rare siderophile elements in localised crustal deposits. The oxidation of these deposits, notably following the Great Oxidation Event, led to an explosion of mineral diversity, with more than 2000 new oxidised mineral species, many of which incorporated chalcophile and siderophile elements.

These deep-time trends in the nature and distribution of mineral-forming ions suggest a plausible paragenetic classification of the elements—a complement to Goldschmidt's geochemical approach that clearly delineated the initial planetary starting point for element classification. Such an effort, placing element and ion distributions in the context of Earth's diverse paragenetic modes, will be the topic of a forthcoming contribution.

In conclusion, minerals continue to provide us with a vivid, information-rich record of Earth's deep-time history. Emerging studies of evolving average fundamental mineral properties such as average symmetry (Bermanec *et al.*, 2024a; 2024b), structural and chemical complexity (Krivovichev *et al.*, 2022), mineral hardness (Bermanec *et al.*, 2023), and chemical composition and oxidation states of mineral-forming ions (e.g. Hummer *et al.*, 2022; Moore *et al.*, 2024a; 2024b), embed a record of global crustal changes tracked through geological time. Thus, minerals represent

an invaluable resource when reconstructing the geological history of our planet.

Dedication

We dedicate this contribution to Professor Edward Grew on the occasion of his 80th birthday. We continue to be inspired by Ed's passion for mineralogy, the integrity and rigor of his research, his tireless advocacy for international cooperation in science, his recognition of the power of informatics to explore complex systems, and his outsized original scientific contributions to our field.

Hallimond Lecture contribution

This publication is submitted in conjunction with the Hallimond Lecture of the Mineralogical Society of Great Britain and Ireland, which was delivered by Robert M. Hazen on 20 August 2024 in Dublin, Ireland at the Fourth European Mineralogical Conference. In a departure from tradition, the awardee is the corresponding author of a contribution with several other scholars, rather than the sole author. This decision reflects both the interdisciplinary nature of the research and the vital role of exceptional early-career scientists in the emerging field of mineral informatics.

Supplementary material. The supplementary material for this article can be found at https://doi.org/10.1180/mgm.2025.10105.

Acknowledgements. We are grateful to Jolyon Ralph for his efforts in developing and disseminating mineral data on https://mindat.org, without which research in mineral informatics would not be possible. We thank two anonymous reviewers, who provided insightful and constructive comments on the penultimate version of this contribution.

Funding statement. Studies of mineral evolution and mineral ecology have been supported by the Deep-time Digital Earth program, the John Templeton Foundation, the NASA Astrobiology Institute ENIGMA team, a private foundation, and the Carnegie Institution for Science. Any opinions, findings, or recommendations expressed herein are those of the authors and do not necessarily reflect the views of the National Aeronautics and Space Administration.

Competing interests. The authors declare none.

References

Aggarwal P.S. and Goswami A. (1961) An oxide of tervalent nickel. The Journal of Physical Chemistry, 65, 2105. https://doi.org/10.1021/j100828a503.

Bermanec M., Eleish A., Morrison S.M., Prabhu A., Wong M.L. and Hazen R.M. (2023) The evolution of mineral hardness reveals both changing parageneses and preservational bias in the mineralogical record. *Minerals*, **13**, 1089. https://doi.org/10.3390/min13081089.

Bermanec M., Vidović N., Gavryliv L., Morrison, S.M. and Hazen R.M. (2024a) Evolution of symmetry index in minerals. *Geoscience Data Journal*, **11**, 69 – 85. https://doi.org/10.1002/gdj3.177.

Bermanec M., Vidović N., Ma X. and Hazen R.M. (2024b) The average symmetry index of minerals co-varies with their hydrogen content, rarity, and paragenetic mode. *Minerals*, 14, 387. https://doi.org/10.3390/min14040387.

Blondel V.D., Guillaume J.-L., Lambiotte R. and Lefebvre E. (2008) Fast unfolding of communities in large networks. *Journal of Statistical Mechanics*, 2008, 1–12. https://doi.org/10.48550/arXiv.0803.0476.

Bostock M., Ogievetsky V. and Heer J. (2011). D³ data-driven documents. *IEEE Transactions on Visualization and Computer Graphics*, 17, 2301–2309. https://doi.org/10.1109/TVCG.2011.185.

Bowen N.L. (1928) The Evolution of the Igneous Rocks. Princeton University Press, New Jersey, USA.

Burke E.A.J. (2006) The end of CNMMN and CCM—Long live the CNMNC! *Elements*, **2**, 388.

- Burnham A.D., Berry A.J., Halse H.R., Schofield P.F., Cibin G. and Mosselmans J.F.W. (2015) The oxidation state of europium in silicate melts as a function of oxygen fugacity, composition and temperature. *Chemical Geology*, 411, 248–259. https://doi.org/10.1016/j.chemgeo.2015.07.002.
- Černý P. (1991) Fertile granites of Precambrian rare-element pegmatite fields: is geochemistry controlled by tectonic setting or source lithologies? Precambrian Research, 51, 429–468. https://doi.org/10.1016/0301-9268(91) 90111-M.
- Chang L.L.Y., Howie R.A. and Zussman J. (1996) Rock-Forming Minerals. Volume 5B, Second Edition. Sulphates, Carbonates, Phosphates and Halides. Longman Group, London.
- Christy A.G. (2015) Causes of anomalous mineralogical diversity in the Periodic Table. *Mineralogical Magazine*, 79, 33–49. https://doi.org/10.1180/minmag.2015.079.1.04.
- Christy A.G. (2018a) Quantifying lithophilicity, chalcophilicity and siderophilicity. European Journal of Mineralogy, 30, 193–204.
- Christy A.G. (2018b) The diversity of mineral species: How many are there, why do some elements form more than others, and how complex can they get? *Australian Journal of Mineralogy*, **19**, 21–33.
- Cooper M.A., Dunning G., Hawthorne F.C., Ma C., Kampf A.R., Spratt J., Stanley C.J. and Christy A.G. (2023) The first occurrence of the carbide anion, C⁴⁻, in an oxide mineral: Mikecoxite, ideally (CHg₄)OCl₂, from the McDermitt open-pit mine, Humboldt County, Nevada, U.S.A. American Mineralogist, 108, 606–613. https://doi.org/10.2138/am-2022-8408.
- Dunning G.E., Hadley T.A., Magnasco J., Christy A.G. and Cooper J.F. Jr. (2005) The Clear Creek mine, San Benito County, California: a unique mercury locality. *The Mineralogical Record*, **36**, 337–363.
- Emsley J. (1991) The Elements, Second Edition. Oxford University Press, New York.
- Fortunato S. (2010) Community detection in graphs. *Physics Reports*, **486**, 75–174. https://doi.org/10.1016/j.physrep.2009.11.002.
- Galili T., O'Callaghan A., Sidi J. and Sievert C. (2018) Heatmaply: An R package for creating interactive cluster heatmaps for online publishing. *Bioinformatics*, 34, 1600–1602. https://doi.org/10.1093/bioinformatics/ btx657.
- Gavryliv L., Ponomar V., Bermanec M. and Putiš M. (2022) The Taxonomy of Mineral Occurrence Rarity and Endemicity. *The Canadian Mineralogist*, 60, 731–758. doi: https://doi.org/10.3749/canmin.2200010.
- Gibbs G.V., Ross N.L., Cox D.F. and Rosso K.M. (2014) Insights into the crystal chemistry of Earth materials rendered by electron density distributions: Pauling's rules revisited. *American Mineralogist*, 99, 1071–1084. https://doi.org/10.2138/am.2014.4660.
- Girvan M. and Newman M.E.J. (2002) Community structure in social and biological networks. *Proceedings of the National Academy of Sciences USA*, **99**, 7821–7826. https://doi.org/10.1073/pnas.122653799.
- Goldschmidt V.M. (1923) Geochemische Verteilungsgesetze der Elemente. Videnskapsselskapets Skrifter. I. Matematisk-naturvidenskapelig klasse, 3, 1, 17
- Goldschmidt V.M. (1937) The principles of distribution of chemical elements in minerals and rocks. The seventh Hugo Müller Lecture, delivered before the Chemical Society on March 17th, 1937. *Journal of the Chemical Society* (resumed), 1937, 655–673. https://doi.org/10.1039/JR9370000655.
- Goldschmidt V.M. (1954) Geochemistry. Oxford University Press, London.
- Greenwood N.N. and Earnshaw A. (1997) Chemistry of the Elements, Second Edition. Butterworth-Heinemann, Oxford, UK.
- Guilbert J.M. and Parks F.P. Jr. (1986) *The Geology of Ore Deposits*. W.H. Freeman, New York.
- Hazen R.M. (2015) Mineral evolution, the Great Oxidation Event and the rise of colorful minerals. *Mineralogical Record*, 46, 805–816, 834.
- Hazen R.M. and Ausubel J.H. (2016) On the nature and significance of rarity in mineralogy. American Mineralogist, 101, 1245–1251. Doi: 10.2138/am-2016-5601
- Hazen R.M. and Morrison S.M. (2020) An evolutionary system of mineralogy, Part I: stellar mineralogy (>13 to 4.6 Ga). *American Mineralogist*, **105**, 627–651. DOI: 10.2138/am-2020-7173.
- Hazen R.M. and Morrison S.M. (2022) On the paragenetic modes of minerals: A mineral evolution perspective. *American Mineralogist*, 107, 1262–1287. https://doi.org/10.2138/am-2022-8099.

Hazen R.M., Mao H.K. and Bell P.M. (1977) Effects of compositional variation on absorption spectra of lunar olivines. *Proceedings of the Lunar Science Conference*, 8, 1081–1090.

- Hazen R.M., Papineau D., Bleeker W., Downs R.T., Ferry J.M., McCoy T.L., Sverjensky D.A. and Yang H. (2008) Mineral evolution. American Mineralogist, 93, 1693–1720. https://doi.org/10.2138/am.2008.2955.
- Hazen R.M., Ewing R.J. and Sverjensky D.A. (2009) Evolution of uranium and thorium minerals. *American Mineralogist*, 94, 1293–1311. https://doi.org/10. 2138/am.2009.3208.
- Hazen R.M., Golden J.J., Downs R.T., Hysted G., Grew E.S., Azzolini D. and Sverjensky D.A. (2012) Mercury (Hg) mineral evolution: A mineralogical record of supercontinent assembly, changing ocean geochemistry and the emerging terrestrial biosphere. *American Mineralogist*, 97, 1013–1042. https://doi.org/10.2138/am.2012.3922.
- Hazen R.M., Jones A.P., Kah L. and Sverjensky D.A. (2013) Carbon mineral evolution. Pp.79–107 in: *Carbon in Earth* (R.M. Hazen, A.P. Jones and J. Baross, editors). Mineralogical Society of America, Washington, DC.
- Hazen R.M., Grew E.S., Downs R.T., Golden J. and Hystad G. (2015) Mineral ecology: Chance and necessity in the mineral diversity of terrestrial planets. *The Canadian Mineralogist*, **53**, 295–323. https://doi.org/10.3749/canmin. 1400086.
- Hazen R.M., Morrison S.M., Prabhu A., Walter M.J. and Williams J.R. (2023a) An evolutionary system of mineralogy, Part VII: The evolution of the igneous minerals (> 2500 Ma). *American Mineralogist*, 108, 1620–1641. https://doi. org/10.2138/am-2022-8539.
- Hazen R.M., Morrison S.M., Prabhu A., Williams J.R., Wong M.L. Krivovichev, S.V. and Bermanec M. (2023b) On the attributes of mineral paragenetic modes. *The Canadian Mineralogist*, 61, 653–673. https://doi.org/10.3749/ 2200022.
- Hummer D.R., Golden J.J., Hystad G., Downs R.T., Eleish A., Liu C., Ralph J., Morrison S.M., Meyer M.B. and Hazen R.M. (2022) Evidence for the oxidation of Earth's crust from the evolution of manganese minerals. *Nature Communications*, 13, 960. https://doi.org/10.1038/s41467-022-285 89-x.
- Hummer D.R., Ma X., Xiang Q., Zhang S., Liu C., Hazen R.M., Golden J.J. and Downs R.T. (2023) A quantitative Goldschmidt ternary classification using correlations of mineral-forming elements. *Geological Society of America* Abstracts with Programs, 55, No. 6. https://doi.org/10.1130/abs/2023AM-395066.
- Ishihara M., Saito Y., Matsumoto F. and Ohba S. (1986) Structures of mercury(I) nitrite and lithium disilver trinitrite. Acta Crystallographica, C42, 1–4. https://doi.org/10.1107/S0108270186097536.
- James M. and Attfield J.P. (1993) The structure and properties of an unusual new nickel(III) oxide: YSr₅Ni₃O₁₁. *Journal of Solid State Chemistry*, **105**, 287–293. https://doi.org/10.1006/jssc.1993.1217.
- Kolaczyk E.D. (2009) Statistical Analysis of Network Data. Springer, New York.
 Krivovichev S.V., Krivovichev V., Hazen R.M., Aksenov S.M., Avdontceva M.S.,
 Banaru A.M., Gorelova L.A., Ismagilova R.M., Kornyakov I.V., Kuporev I.V.,
 Morrison S.M Panikorovskii T.L. and Starova G.L. (2022) Structural and chemical complexity of minerals: An update. Mineralogical Magazine, 86, 183–204. https://doi.org/10.1180/mgm.2022.23.
- Lafuente B., Downs R.T., Yang H. and Stone N. (2015) The power of databases: the RRUFF project. Pp. 1–30 in: *Highlights in Mineralogical Crystallography* (Armbruster T. and Danisi R.M., editors). W. De Gruyter, Berlin.
- Leclaire A. and Raveau B. (1988) Small atomic displacements in the molybdenophosphates AP_3O_{12} (A=K, Rb, Tl). Acta Crystallographica, 44, 226–229
- Letard I., Sainctvit P. and Deudon C. (2007) XMCD at Fe L2,3 edges, Fe and S K edges in Fe₇S₈. *Physics and Chemistry of Minerals*, **34**, 113–120. https://doi.org/10.1007/s00269-006-0132-8.
- Liu C., Hystad G., Golden J.J., Hummer D.R., Downs R.T., Morrison S.M., Grew E.S. and Hazen R.M. (2017) Chromium mineral ecology. *American Mineralogist*, 102, 612–619. https://doi.org/10.2138/am-2017-5900.
- Liu C., Eliesh A., Hystad G., Golden J.J., Downs R.T., Morrison S.M., Hummer D.R., Ralph J.P., Fox P. and Hazen R.M. (2018) Analysis and visualization of vanadium mineral diversity and distribution. *American Mineralogist*, **103**, 1080–1086. https://doi.org/10.2138/am-2018-6 274.

- Lodders K. and Hazen R.M. (2026) Goldschmidt's geochemical classification of the elements revisited: The evolution of a nuanced hypothesis. American Mineralogist, in press. https://doi.org/10.2138/am.2025.9788
- London D. (2008) Pegmatites. Mineralogical Association of Canada, Canada. Maimon O. and Rokarch L. (2006) Clustering methods. Pp. 321–352 in: Data Mining and Knowledge Discovery Handbook. Springer, New York.
- Marks M.A.W. and Markl G. (2017) A global review on agpaitic rocks. Earth Science Reviews, 173, 229–258. https://doi.org/10.1016/j.earscirev.2017.06. 002.
- Martin R.F. and Wüsler P.-A. (2014) Niobium and tantalum in minerals: Siderophile, chalcophile or lithophile, and polyvalent. *Journal of Geochemical Exploration*, **147**(A), 16–25. https://doi.org/10.1016/j.gexplo.2014.05.006.
- Mills S.J., Hatert F., Nickel E.H. and Ferrais G. (2009) The standardization of mineral group hierarchies: Application to recent nomenclature proposals. *European Journal of Mineralogy*, **21**, 1073–1080. https://doi.org/10.1127/0935-1221/2009/0021-1994.
- Mitchell R.H. (editor) (1996a) Undersaturated Alkaline Rocks: Mineralogy, Petrogenesis and Economic Potential. Mineralogical Association of Canada, Short Course, 24.
- Mitchell R.H. (1996b) Classification of undersaturated and related alkaline rocks. *Mineralogical Association of Canada Short Course*, **24**, 1–22.
- Moore E.K., Golden J.J., Morrison S.K., Hao J. and Spielman S.J. (2022) The expanding network of mineral chemistry throughout earth history reveals global shifts in crustal chemistry during the Proterozoic. *Scientific Reports*, 12, 4956. https://doi.org/10.1038/s41598-022-08650-x.
- Moore E.K., Diedolf J.E., Morrison S.M. and Hummer D.R. (2024a) Characterizing sulfur redox state and geochemical implications in deeptime using mineral chemistry network analysis. *Geochimica et Cosmochimica Acta*, 376, 25–36. https://doi.org/10.1016/j.gca.2024.05.024.
- Moore E.K., Li J., Zhang A., Hao J., Morrison S.M., Hummer D.R. and Yee N. (2024b) Uranium redox and deposition transitions embedded in deep-time geochemical models and mineral chemistry networks. *Geochemistry, Geophysics, Geosystems*, 25, e2023GC011267. https://doi.org/10.1029/2023GC011267.
- Morrison S.M. and Hazen R.M. (2020) An evolutionary system of mineralogy, Part II: Interstellar and solar nebula primary condensation mineralogy (> 4.565 Ga). *American Mineralogist*, **105**, 1508–1535. https://doi.org/10.2138/am-2020-7447.
- Morrison S.M., Liu C., Eleish A., Prabhu A., Li C., Ralph J., Downs R.T., Golden J.J., Fox P., Hummer D.R., Meyer M.B. and Hazen R.M. (2017) Network analysis of mineralogical systems. *American Mineralogist*, **102**, 1588–1596. https://doi.org/10.2138/am-2017-6104.
- Morrison S.M., Prabhu A. and Hazen R.M. (2024) An evolutionary system of mineralogy. Part VIII. The evolution of metamorphic minerals. *American Mineralogist*, 109, 1760–1784. https://doi.org/10.2138/am-2023-9004.
- Newman M.E.J. (2013) Networks: An Introduction. Oxford University Press, New York.
- O'Driscoll B. and Van Tongeren J.A. (2017) Layered intrusions: From petrological paradigms to precious metal repositories. *Elements*, 13, 383–389. https://doi.org/10.2138/gselements.13.6.383.
- Pauling L. (1932) The nature of the chemical bond. IV. The energy of single bonds and the relative electronegativity of atoms. *Journal of the American Chemical Society*, 54, 3570–3582. https://doi.org/10.1021/ja01348a011.

- Pauling L. (1960) The Nature of the Chemical Bond and the Structure of Molecules and Crystals. Cornell University Press, Ithaca NY, USA.
- Pearce C.I., Pattrick R.A.D., Vaughan D.J., Henderson C.M.B. and van der Laan G. (2006) Copper oxidation state in chalcopyrite: Mixed Cu d9 and d10 characteristics. *Geochimica et Cosmochimica Acta*, 70, 4635–4642. https://doi.org/10.1016/j.gca.2006.05.017.
- Pirajno F. (2009) *Hydrothermal Processes and Mineral Systems*. Springer Science, Berlin, Germany.
- Plotly Technologies Inc. (2015) Collaborative data science. Montréal, QC, Canada, https://plot.ly.
- Pons P. and Latapy M. (2005). Computing communities in large networks using random walks. *Proceedings*, 20, 284–293. Computer and Information Sciences-ISCIS 2005, 20th International Symposium, Istanbul, Turkey, October 26–28, 2005, Springer Berlin Heidelberg.
- Poot J., Buelens P., Dekoninck A., Rochez G. and Yans J. (2024) Tracing the Eh-pH evolution of Cu-Pb-As-Zn supergene mineralization using detailed petrography in the Cap Garonne mineral deposit (Provence, France). *Mineralium Deposita*, 59, 1249–1271. https://doi.org/10.1007/s00126-024-01258-3.
- Que X., Huang J., Ralph J., Zhang J., Prabhu A., Morrison S., Hazen R.M. and Ma X. (2024). Using adjacency matrix to explore remarkable associations in big and small mineral data. *Geoscience Frontiers*, 15, 101823. https://doi.org/ 10.1016/j.gsf.2024.101823.
- Sawyer J.F. and Schrobilgen G.J.D. (1982) Tris(pentafluorotellurato(VI))boron(III). *Acta Crystallographica B*, **38**, 1561–1563. https://doi.org/10.1107/S0567740882006384.
- Schertl H.-P., Mills S.J. and Maresch W.V. (2018) A Compendium of IMA-Approved Mineral Nomenclature. International Mineralogical Association, Schweizerbart'sche Verlagsbuchhandlung, Stuttgart, Germany.
- Touchard V., Louer M., Auffredic J.P. and Louer D. (1987) Polymorphisme de l'iodure de cesium et de cadmium. Revue de Chimie Minerale, 24, 414– 426
- Weill D.F. and Drake M.J. (1973) Europium anomaly in plagioclase feldspar: Experimental results and semiquantitative model. *Science*, **180**, 1059–1060. https://doi.org/10.1126/science.180.4090.1059.
- Welch M.D., Hawthorne F.C., Cooper M.A. and Kyser T.K. (2001) Trivalent iodine in the crystal structure of schwartzembergite, Pb²+₃I³+O₆H₂Cl₃. *The Canadian Mineralogist*, **39**, 785–795. https://doi.org/10.2113/gscanmin.39. 3.785.
- Wood B.J. and Kiseeva E.S. (2015) Trace element partitioning into sulfide: How lithophile elements become chalcophile and vice versa. American Mineralogist, 100, 2371–2379. https://doi.org/10.2138/am-2015-5358.
- Zhang J., Que X., Madhikarmi B., Hazen R. M., Ralph J., Prabhu A., Morrison S. and Ma X. (2024). Using a 3D heat map to explore the diverse correlations among elements and mineral species. *Applied Computing and Geosciences*, 21, 100154. https://doi.org/10.1016/j.acags.2024.100154.
- Zhuang Z., Zhang Y.,Li Y., Yin R., Li C., Lu A., Lai Y., Bai X., Wang C. and Jia H. (2024) Evolutionary dynamics of redox-sensitive minerals reveal details and possible regulatory mechanisms of Earth's oxygenation events. Earth and Planetary Science Letters, 626, 118528. https://doi.org/10.1016/j.epsl.2023. 118528Get rights and content.